

## Resonantly Detecting Axion-Mediated Forces with Nuclear Magnetic Resonance

Asimina Arvanitaki<sup>1</sup> and Andrew A. Geraci<sup>2,\*</sup>

<sup>1</sup>*Perimeter Institute for Theoretical Physics, Waterloo, Ontario N2L 2Y5, Canada*

<sup>2</sup>*Department of Physics, University of Nevada, Reno, Nevada 89557, USA*

(Received 5 March 2014; revised manuscript received 27 August 2014; published 14 October 2014)

We describe a method based on precision magnetometry that can extend the search for axion-mediated spin-dependent forces by several orders of magnitude. By combining techniques used in nuclear magnetic resonance and short-distance tests of gravity, our approach can substantially improve upon current experimental limits set by astrophysics, and probe deep into the theoretically interesting regime for the Peccei-Quinn (PQ) axion. Our method is sensitive to PQ axion decay constants between  $10^9$  and  $10^{12}$  GeV or axion masses between  $10^{-6}$  and  $10^{-3}$  eV, independent of the cosmic axion abundance.

DOI: 10.1103/PhysRevLett.113.161801

PACS numbers: 14.80.Va, 76.60.-k, 13.40.Em

*Introduction.*—Axions are  $CP$ -odd scalar particles that are present in a variety of theories beyond the standard model. Their mass is protected by shift symmetries so they remain naturally light and their couplings to matter are very suppressed. In string theory in particular, they naturally arise in compactifications with nontrivial topology [1,2], and their mass can be as small as the Hubble scale. The most famous axion is the Peccei-Quinn (PQ) axion [3] whose presence explains the smallness of the neutron's electric dipole moment and has been the main focus of experimental searches since it was proposed over 30 years ago. Its mass is generated by nonperturbative QCD effects. If lighter than  $10^{-5}$  eV, the PQ axion becomes an excellent dark matter candidate. In laboratory experiments, axions can generate novel spin-dependent short-range forces between matter objects [4].

In this Letter, we propose a magnetometry experiment based on nuclear magnetic resonance (NMR) that searches for axion mediated  $CP$ -violating forces with a range between  $\sim 100$   $\mu\text{m}$  and  $\sim 10$  cm or axion masses between  $\sim 10^{-6}$  eV and  $\sim 10^{-3}$  eV. Our proposal is based on the resonant coupling between the rotational frequency of a source mass and a NMR sample with a matching spin precession frequency. Similar techniques involving resonant excitation are used in short-distance gravity experiments [5–7]. In the presence of an anomalous  $CP$ -violating interaction with the source mass, the spins in the NMR material will resonantly precess off the axis of polarization. This can be measured with a superconducting quantum interference device (SQUID).

There are already several methods based on precision magnetometry to look for such spin-dependent short range forces, see for example Refs. [8–11] (for a summary of recent results see Ref. [12]). In previous experiments, shifts of the spin-precession frequency were observed as matter objects were brought into and out of proximity with a sample. Our setup is different from previous approaches as the detection technique is based on a resonant effect, where

the source mass *itself* is moved periodically at the Larmor frequency in order to drive spin precession in the NMR medium. This helps reduce several systematics while taking advantage of the enhancement of the signal due to the high spin density of the NMR material ( $\sim 10^{21}$   $\text{cm}^{-3}$ ) and the quality factor of the NMR sample which can be as high as  $10^6$ .

In the following, we show how the proposed setup can probe both the monopole-dipole and the dipole-dipole coupling of axions at a level that is competitive with astrophysical bounds. The experiment can eventually be up to 8 orders of magnitude more sensitive than current approaches and can bridge the gap between astrophysical bounds and cosmic PQ axion searches [13,14], without requiring that the axion is dark matter or the need to precisely scan over its mass.

*Axion-mediated forces.*—The interaction energy between particles due to monopole-dipole axion exchange as a function of the distance  $r$  is [4]

$$U_{sp}(r) = \frac{\hbar^2 g_s g_p}{8\pi m_f} \left( \frac{1}{r\lambda_a} + \frac{1}{r^2} \right) e^{-(r/\lambda_a)} (\hat{\sigma} \cdot \hat{r}), \quad (1)$$

where  $m_f$  is the fermion mass, or in the case of dipole-dipole axion exchange

$$U_{pp}(r) = \frac{\hbar^3 c}{16\pi m_{f_1} m_{f_2}} \left[ (\hat{\sigma}_1 \cdot \hat{\sigma}_2) \left( \frac{1}{r^2 \lambda_a} + \frac{1}{r^3} \right) e^{-(r/\lambda_a)} - (\hat{\sigma}_1 \cdot \hat{r})(\hat{\sigma}_2 \cdot \hat{r}) \left( \frac{1}{r\lambda_a^2} + \frac{3}{r^2 \lambda_a} + \frac{3}{r^3} \right) e^{-(r/\lambda_a)} \right]. \quad (2)$$

The range of interaction is set by the mass of the axion by  $\lambda_a = h/m_a c$ . It is convenient to write these interactions that involve spins (i.e., dipoles) using the axion potentials  $V_{a_s}(r)$  and  $V_{a_p}(r)$ , where

$$\begin{aligned} U_{sp}(r) &= -\vec{\nabla}V_{a_s}(r) \cdot \hat{\sigma}_2, \\ U_{pp}(r) &= -\vec{\nabla}V_{a_p}(r) \cdot \hat{\sigma}_2. \end{aligned} \quad (3)$$

Here  $V_{a_s}(r) = (\hbar^2 g_s g_p / 8\pi m_f) (e^{-(r/\lambda_a)} / r)$  for monopole-dipole interactions, or  $V_{a_p}(r) = (\hbar^3 c / 16\pi) (g_{p_1} g_{p_2} / m_{f_1} m_{f_2}) (\hat{\sigma}_1 \cdot \hat{r}) ((1/r^2) + (1/\lambda_a r)) e^{-(r/\lambda_a)}$ , if an axion can be exchanged between two spins. Equation (3) shows the axion generated potential by an unpolarized or polarized mass acts on a nearby fermion as an “effective” magnetic field

$$\vec{B}_{\text{eff}} = \frac{2\vec{\nabla}V_a(r)}{\hbar\gamma_f}, \quad (4)$$

where  $\gamma_f$  is the fermion gyromagnetic ratio, and we omit the subscripts in  $V_{a_s}$  and  $V_{a_p}$  for brevity. However, this field is different from an ordinary electromagnetic field—it couples to the spin of the particle, is independent of the fermion’s magnetic moment, and does not couple to electric charge, moving charges, or ordinary angular momentum. As the axion potential is generated by pseudoscalar exchange rather than vector gauge boson (i.e., photon) exchange,  $\vec{B}_{\text{eff}}$  is not subject to Maxwell’s equations. Therefore, it crucially is not screened by magnetic shielding.

For the PQ axion  $g_s$  and  $g_p$  satisfy

$$6 \times 10^{-27} \left( \frac{10^9 \text{ GeV}}{f_a} \right) \lesssim g_s \lesssim 10^{-21} \left( \frac{10^9 \text{ GeV}}{f_a} \right), \quad (5)$$

$$g_p = \frac{C_f m_f}{f_a} = C_f 10^{-9} \left( \frac{m_f}{1 \text{ GeV}} \right) \left( \frac{10^9 \text{ GeV}}{f_a} \right), \quad (6)$$

where  $m_a = 6 \times 10^{-3} \text{ eV} (10^9 \text{ GeV} / f_a)$ .  $g_s$  is indirectly constrained from above by electric dipole moment searches and the lower bound is set by the amount of  $CP$  violation in the standard model [15,16]. There are large uncertainties in the QCD matrix elements involved in the calculations of this coupling and further study is required through lattice simulations.  $C_f$  is a model dependent constant typically expected to be  $\mathcal{O}(1)$  [17] and in what follows we assume  $C_f = 1$  for simplicity. The axion decay constant is constrained to be  $10^9 \text{ GeV} \lesssim f_a \lesssim 10^{17} \text{ GeV}$  by astrophysics; the lower bound comes from red giant cooling and SN 1987a, while the lesser known upper bound on  $f_a$  arises because the wavelength of a large  $f_a$  PQ axion is of order the size of stellar mass black holes. If such an axion existed, these black holes would spin down through the super-radiance effect [2,18]. They are thus excluded by observations of near extremal black holes.

*Experimental setup.*—The setup is schematically drawn in Fig. 1. A quartz vessel containing hyperpolarized  $^3\text{He}$  gas is placed next to a segmented cylinder or radius  $R$  that

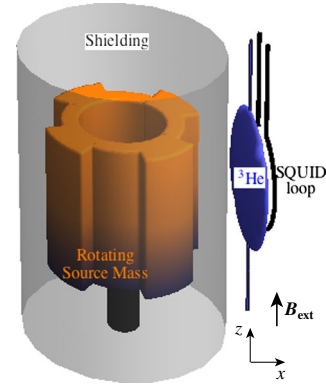


FIG. 1 (color online). A source mass consisting of a segmented cylinder with  $n$  sections is rotated around its axis of symmetry at frequency  $\omega_{\text{rot}}$ , which results in a resonance between the frequency  $\omega = n\omega_{\text{rot}}$  at which the segments pass near the sample and the resonant frequency  $2\vec{\mu}_N \cdot \vec{B}_{\text{ext}} / \hbar$  of the NMR sample. Superconducting cylinders screen the NMR sample from the source mass and (not shown) the setup from the environment.

acts as a source mass. The cylinder consists of either high density unpolarized material (e.g., tungsten) or material with a net electron or nuclear spin polarization, and is rotated around its axis of symmetry with a frequency  $\omega_{\text{rot}}$ . To screen background electromagnetic fields including surface magnetic field noise [19], a superconducting Nb shell is placed between the cylinder and  $^3\text{He}$  sample.

An axion with  $\lambda_a < R$  will generate a potential at a distance  $r \ll R$  from the surface of the cylinder approximately given by  $V_a(r) \approx (\hbar^2 g_s g_{p_N} / 2m_N) \lambda_a^2 n_N e^{-(r/\lambda_a)}$ , if the axion has a monopole coupling to nucleons, and  $m_N$  and  $n_N$  are the nucleon mass and density of the material, respectively, or  $V_a(r) \approx (\hbar^3 c g_{p_f} g_{p_N} / 4m_f m_N) \lambda_a n_p e^{-(r/\lambda_a)}$ , if the axion has a dipole coupling to nucleons or to electrons and the polarization of the source mass is perpendicular to the axis of rotation, where  $n_p$  is the polarized spin density in the material. Here we assume the cylinder surface is effectively flat. For our sensitivity estimates we numerically integrate over the actual dimensions of the cylinder. Given the proximity of the sample, nonflatness affects the overall signal by less than 10%. We also assume the NMR sample thickness is of order  $\lambda_a$ .

A spin polarized nucleus near this rotating segmented cylinder will feel an effective magnetic field of approximately

$$\vec{B}_{\text{eff}} \approx \frac{1}{\hbar\gamma_N} \nabla V_a(r) [1 + \cos(n\omega_{\text{rot}}t)], \quad (7)$$

where  $\gamma_N$  is the nuclear gyromagnetic ratio and  $n$  is the number of segments.  $\vec{B}_{\text{eff}}$  is parallel to the radius of the cylinder. The exact time-varying field can be determined by numerical integration over the cylinder geometry. From the Bloch equations, a NMR sample with net polarization  $M_z$

parallel to the axis of the cylinder (and a Larmor frequency  $2\vec{\mu}_N \cdot \vec{B}_{\text{ext}}/\hbar = \omega$  determined by an axial field  $\vec{B}_{\text{ext}}$ ) will develop a time-varying perpendicular magnetization  $M_x$  in response to the resonant effective axion field  $B_{\text{eff}}$ :

$$M_x(t) \approx \frac{1}{2} n_s p \mu_N \gamma N B_{\text{eff}} T_2 (e^{-t/T_1} - e^{-t/T_2}) \cos(\omega t), \quad (8)$$

where  $p$  is the polarization fraction,  $n_s$  is the spin density in the sample, and  $\mu_N$  is the nuclear magnetic moment.  $M_x(t)$  grows approximately linearly with time until  $t \sim T_2$ , the transverse relaxation time, and then decays at the longer longitudinal relaxation time  $T_1$ .  $M_x(t)$  can be detected by a SQUID with its pickup coil axis oriented radially.

The main fundamental limitation comes from transverse projection noise in the sample itself  $\sqrt{M_N^2} = \sqrt{(\hbar \gamma n \mu_{^3\text{He}} T_2 / 2V)}$  and the minimum transverse magnetic resonant field this setup is sensitive to is given by

$$B_{\text{min}} \approx p^{-1} \sqrt{\frac{2\hbar b}{n_s \mu_{^3\text{He}} \gamma V T_2}} = 3 \times 10^{-19} \text{T} \left(\frac{1}{p}\right) \times \sqrt{\left(\frac{b}{1 \text{ Hz}}\right) \left(\frac{1 \text{ mm}^3}{V}\right) \left(\frac{10^{21} \text{ cm}^{-3}}{n_s}\right) \left(\frac{1000 \text{ s}}{T_2}\right)}. \quad (9)$$

Here  $V$  is the sample volume,  $\gamma$  is the gyromagnetic ratio for  $^3\text{He}$  ( $= (2\pi) \times 32.4 \text{ MHz/T}$ ),  $b$  is the measurement bandwidth, and  $\mu_{^3\text{He}} = -2.12 \times \mu_n$  is the  $^3\text{He}$  nuclear moment [20]. Equation (9) shows where the tremendous boost in sensitivity lies. First, resonant enhancement improves the sensitivity due to an effective quality factor  $Q = \omega T_2$ , and second there is a gain by the large number of nuclei  $n_s V$  simultaneously being observed. We choose  $^3\text{He}$  because it has a long coherence time ( $T_2 \approx 1000 \text{ s}$  for the liquid state) and  $p \approx 1$  has already been achieved with optical pumping techniques [21].

*Monopole-dipole axion exchange.*—For concreteness, we consider a tungsten cylindrical shell of length 1 cm, thickness 4 mm, and outer diameter 3.8 cm divided into 20 sections of length 6 mm. The radius of each section is modulated by  $200 \mu\text{m}$  in order to generate a time-varying potential at frequency  $\omega = 10 \omega_{\text{rot}}$ , due to the difference in the axion-mediated interaction as each section passes by the sensor. The rotation of the cylinder can be accomplished by an in-vacuum piezoelectric transducer [22]. To decouple mechanical vibration,  $\omega_{\text{rot}} \ll \omega$ .

The  $^3\text{He}$  sample fills a quartz spheroidal enclosure of internal diameters  $3 \text{ mm} \times 3 \text{ mm} \times 150 \mu\text{m}$ . For this sample,  $B_{\text{min}} = 3 \times 10^{-19} \text{ (T}/\sqrt{\text{Hz}})$  for  $T_2 = 1000 \text{ s}$ . For proximity of the source mass, we assume a  $25 \mu\text{m}$  thick stretched  $1 \text{ cm} \times 1 \text{ cm}$  niobium foil screen covers a cutaway region of the shield between the mass and sample.

The  $^3\text{He}$  vessel has wall thickness  $50 \mu\text{m}$  and is rigidly attached to the shield to minimize their relative motion. The gap between the shield and rotating mass is  $50 \mu\text{m}$ .

The sample and source mass are housed in a He cryostat. An outer niobium shield enclosing the apparatus screens stray background magnetic fields. The rotational mechanism can be thermally shielded and heated. If  $\omega_{\text{rot}}/2\pi = 10 \text{ Hz}$  and  $\omega/2\pi$  is  $100 \text{ Hz}$ , then the net  $B_{\text{ext}}$  needed at the sample is  $\sim 30 \text{ mG}$ .  $B_{\text{ext}}$  is the sum of the internal field of the sample ( $\sim 0.2 \text{ G}$  for  $n_s = 2 \times 10^{21} \text{ cm}^{-3}$ ) and a field generated by superconducting coils.

In Fig. 2 we present the reach of the setup for an integration time of  $10^6 \text{ s}$  for a monopole-dipole axion mediated interaction for both  $T_2 = 1 \text{ s}$  and  $1000 \text{ s}$ . Since the phase of rotation of the driving mass can be recorded, the integration time need not be continuous, allowing repolarization of the gas between experimental runs. The limitation is due to noise indicated in Eq. (9), which lies significantly above the SQUID sensitivity. For example, with  $B_{\text{eff}} = 3 \times 10^{-19} \text{ T}$  at  $100 \text{ Hz}$ , the signal at the SQUID due to  $M_x$  will be  $\sim 10^{-15}$  to  $10^{-12} \text{ T}$  for  $T_2 = 1$  to  $1000 \text{ s}$ , respectively. We also include a future projection of ultimate limits by scaling the size of the apparatus and increasing the sample density to that of liquid  $^3\text{He}$ . In this case, we divide our projection into two regions: for axions with  $\lambda_a < 1 \text{ mm}$  we assume that the sample area cannot be larger than  $10^4 \times \lambda_a^2$ , while it is fixed to  $100 \text{ cm}^2$  for lighter axions. Experimental parameters are in Table I. Finally, we

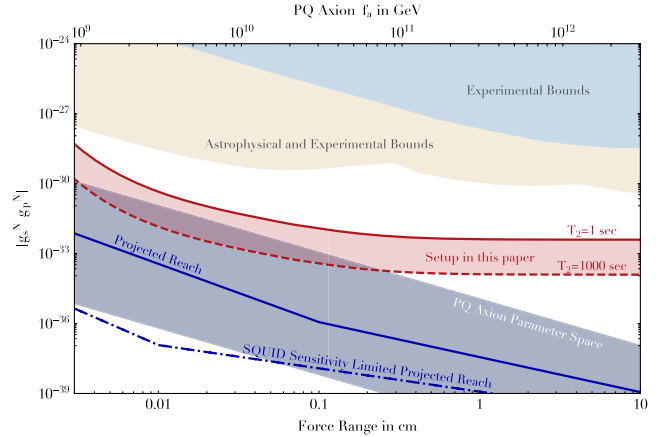


FIG. 2 (color online). Projected reach for monopole-dipole axion mediated interactions. The band bounded by the red (dark) solid line and dashed line denotes the limit set by transverse magnetization noise for the specific setup described in the text, for  $T_2$  ranging from 1 s to 1000 s. The blue (darker) solid line is a future projection obtained by scaling the setup using parameters chosen in Table 1. The blue (darker) dot-dashed line is the projected limit set by the SQUID sensitivity in a scaled setup. The integration time in all setups is  $10^6 \text{ s}$ . The shaded band is the parameter space for the PQ axion with  $C_f = 1$ . Experimental as well as combined experimental and astrophysical bounds are also presented [9–12].

TABLE I. Experimental parameters for the setup described in the text and the ultimate projected sensitivity of the setup used in our estimates shown in Figs. 2 and 3.

Source mass	Unpolarized	Polarized
W nucleon density	$184 \times (6.4 \times 10^{22}) \text{ cm}^{-3}$	
Xe spin density		$2 \times 10^{22} \text{ cm}^{-3}$
Fe spin density		$8 \times 10^{22} \text{ cm}^{-3}$
NMR sample	Setup in this Letter	Projected
V ( $\lambda_a > 1 \text{ mm}$ )	$(3 \text{ mm})^2 \times 150 \mu\text{m}$	$10^2 \text{ cm}^2 \times \lambda_a$
( $\lambda_a < 1 \text{ mm}$ )	$(3 \text{ mm})^2 \times 150 \mu\text{m}$	$10^4 \lambda_a^2 \times \lambda_a$
$T_2$	1–1000 sec	1000 sec
$p$	1	1
$n_s$	$2 \times 10^{21} \text{ cm}^{-3}$	$2 \times 10^{22} \text{ cm}^{-3}$
SQUID	$1.5(fT/\sqrt{\text{Hz}})$	$0.15(fT/\sqrt{\text{Hz}})$
( $\lambda_a < 0.1 \text{ mm}$ )		$(1 \text{ cm}^2/10^4 \lambda_a^2)$
( $\lambda_a > 0.1 \text{ mm}$ )	$1.5(fT/\sqrt{\text{Hz}})$	$0.15(fT/\sqrt{\text{Hz}})$

show the PQ axion parameter space assuming  $C_f = 1$  as well as astrophysical or experimental bounds [12]. Not only does the proposed setup compete with astrophysical bounds, but it probes a large part of the traditional axion window of  $10^9 \text{ GeV} < f_a < 10^{12} \text{ GeV}$ .

In order for the full sample to remain on resonance, gradients across the sample need to be controlled at the level of  $\sim 10^{-11} (1000 \text{ s}/T_2)$  T. The spheroidal shape of the sample suppresses magnetic gradients due to the magnetized gas itself. However, gradients result from image currents arising from the Meissner effect in the Nb shield. To minimize the effects of gradients, the  $^3\text{He}$  vessel can be extended to 1 cm in the  $z$  direction, while the active region remains 3 mm in size. Finite element simulations indicate that the gradient is controlled in this central region at the level of  $5 \times 10^{-8}$  T, which left unchecked will limit  $T_2$  to  $\sim 1$  s for the gas density we consider. A superconducting coil setup can also partially cancel the gradient, allowing extension of  $T_2$  up to 100 s for a 99% compensation. However, diffusion of the gas from the central active region to and from the surrounding gradient compensation region can also contribute to decoherence as  $\exp[-D(\gamma\nabla_z B)^2(t^3/3)]$ , where  $D$  is the diffusion constant [23]. Taking  $D = 1.7 \times 10^{-3} \text{ cm}^2/\text{s}$ , to diffuse by 3 mm takes approximately 100 s. Thus to avoid significant mixing between the active sample region and surrounding region with larger gradients, with a 99% gradient compensation, the effective  $T_2$  is reduced to  $\sim 10$  s. In principle spin-echo techniques could also be employed to further reduce the effects of gradients, as in Ref. [24].

Acoustic vibrations can cause magnetic field variations due to the image magnetization in the shields. Assuming a  $10 \mu\text{m}$  wobble in the cylinder at  $\omega_{\text{rot}}/2\pi = 10 \text{ Hz}$  and 1% at 100 Hz, we estimate  $\delta_x \sim 2 \text{ nm}$  of relative motion between the sample and outer shield. This results in a resonant field  $\sim 10^{-22}$  T. Relative motion between the

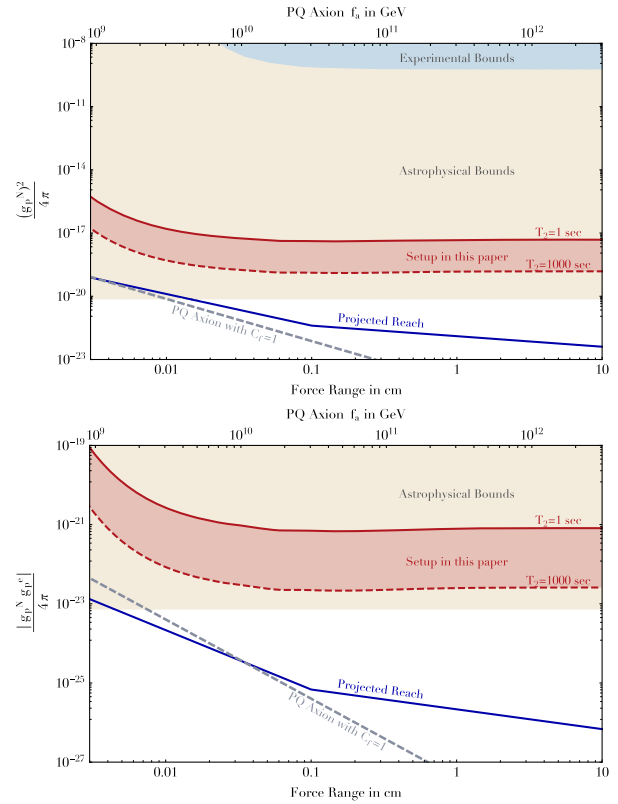


FIG. 3 (color online). Reach for dipole-dipole mediated interactions between  $^3\text{He}$  nuclei (top) or electrons and  $^3\text{He}$  nuclei (bottom). The red (dark) solid and dashed lines denote the limits set by the source mass described in the text or a liquid  $^3\text{He}$  sample with  $T_2 = 1$  and 1000 s, respectively. The ultimate projected sensitivity is the blue (darker) solid line. The integration time is  $10^6$  s. Also shown are the PQ axion signal for  $C_f = 1$  and astrophysical or experimental bounds from Ref. [12].

sample and shield to which it is rigidly attached produces a similar field. When the shield is cooled at low fields ( $< 10^{-10}$  T) we estimate trapped fluxes to be less than  $10 \text{ cm}^{-2}$ . The thermal noise from a trapped flux at distance  $r$  from the sample is [25,26]  $7 \times 10^{-20} (T/\sqrt{\text{Hz}}) (200 \mu\text{m}/r)^3$ . For  $\delta_x = 2 \text{ nm}$ , this background is  $\lesssim 10^{-22}$  T.

The Barnett effect [27] can produce a resonant background magnetic field of  $\sim 10^{-14}$  T. This background is eliminated by a shield with a screening factor  $> 10^5$ . This is possible for thin shielding layers ( $\sim 10 \mu\text{m}$ ), by appropriately choosing the shield length. The shield also attenuates magnetic noise due to thermal currents in the tungsten mass [19], which we estimate at  $10^{-12} \text{ T}/\sqrt{\text{Hz}}$ .

*Dipole-dipole axion exchange.*—Using a spin-polarized source mass requires additional superconducting and  $\mu$ -metal shielding, and requires special consideration when probing sub-200  $\mu\text{m}$  distances. The ultimate reach of such a setup is estimated in Fig. 3.

*Discussion.*—Additional control of systematics is possible by placing more than one detector around the source mass, and testing for correlations in their signals. Specially

shaped shields could reduce gradients due to the Meissner effect. Using different NMR materials could test different nucleon interactions. Besides axions, this technique can also be used for light gauge boson searches. Most importantly, this technique enables probing the PQ axion parameter space in the traditional axion window of  $f_a$  between  $10^9$  and  $10^{12}$  GeV, bridging the gap between astrophysical bounds and cosmic axion searches.

We are grateful to S. Dimopoulos, B. Cabrera, and M. Romalis for useful discussions and feedback. We also thank A. Kapitulnik, E. Levinson-Falk, and B. Lev for their insight. We thank J. Stutz for finite element simulations. A. A. is thankful to D. Cory, P. Graham, J. March-Russell, M. Pospelov, and G. Villadoro. A. G. is supported by Grant No. NSF PHY-1205994. A. A. was partially supported by ERC Grant BSMOXFORD No. 228169. Research at Perimeter Institute is supported by the Government of Canada through Industry Canada and by the Province of Ontario through the Ministry of Economic Development and Innovation.

---

\*Corresponding author.  
ageraci@unr.edu

- [1] P. Svrcek and E. Witten, *J. High Energy Phys.* **06** (2006) 051.
- [2] A. Arvanitaki, S. Dimopoulos, S. Dubovsky, N. Kaloper, and J. March-Russell, *Phys. Rev. D* **81**, 123530 (2010).
- [3] R. D. Peccei and H. R. Quinn, *Phys. Rev. Lett.* **38**, 1440 (1977); S. Weinberg, *Phys. Rev. Lett.* **40**, 223 (1978); F. Wilczek, *Phys. Rev. Lett.* **40**, 279 (1978).
- [4] J. E. Moody and F. Wilczek, *Phys. Rev. D* **30**, 130 (1984).
- [5] A. A. Geraci, S. J. Smullin, D. M. Weld, J. Chiaverini, and A. Kapitulnik, *Phys. Rev. D* **78**, 022002 (2008).
- [6] D. J. Kapner, T. S. Cook, E. G. Adelberger, J. H. Gundlach, B. R. Heckel, C. D. Hoyle, and H. E. Swanson, *Phys. Rev. Lett.* **98**, 021101 (2007).
- [7] J. C. Long, H. W. Chan, A. B. Churnside, E. A. Gulbis, M. C. M. Varney, and J. C. Price, *Nature (London)* **421**, 922 (2003).
- [8] G. Vasilakis, J. M. Brown, T. W. Kornack, and M. V. Romalis, *Phys. Rev. Lett.* **103**, 261801 (2009).
- [9] K. Tullney *et al.*, *Phys. Rev. Lett.* **111**, 100801 (2013).
- [10] P.-H. Chu *et al.*, *Phys. Rev. D* **87**, 011105(R) (2013).
- [11] M. Bulatowicz, R. Griffith, M. Larsen, J. Mirijanian, C. B. Fu, E. Smith, W. M. Snow, H. Yan, and T. G. Walker, *Phys. Rev. Lett.* **111**, 102001 (2013).
- [12] G. Raffelt, *Phys. Rev. D* **86**, 015001 (2012).
- [13] S. J. Asztalos *et al.*, *Phys. Rev. Lett.* **104**, 041301 (2010).
- [14] D. Budker, P. W. Graham, M. Ledbetter, S. Rajendran, and A. Sushkov, *Phys. Rev. X* **4**, 021030 (2014).
- [15] M. Pospelov, *Phys. Rev. D* **58**, 097703 (1998); *Phys. Lett. B* **530**, 123 (2002); M. Pospelov and A. Ritz, *Ann. Phys. (Amsterdam)* **318**, 119 (2005).
- [16] M. Pospelov (private communication).
- [17] J. Beringer *et al.* (Particle Data Group Collaboration), *Phys. Rev. D* **86**, 010001 (2012).
- [18] A. Arvanitaki and S. Dubovsky, *Phys. Rev. D* **83**, 044026 (2011).
- [19] T. Varpula and T. Poutanen, *J. Appl. Phys.* **55**, 4015 (1984).
- [20] J. L. Flowers, B. W. Petley, and M. G. Richards, *Metrologia* **30**, 75 (1993).
- [21] T. Ino and S. Muto, *Physica (Amsterdam)* **397B**, 182 (2007); R. H. Romer, *Phys. Rev.* **117**, 1183 (1960).
- [22] Pi Corporation, [www.Pi.ws](http://www.Pi.ws).
- [23] M. Himbert, J. Dupont-Roc, and C. Lhuillier, *Phys. Rev. A* **39**, 6170 (1989).
- [24] M. P. Ledbetter, I. M. Savukov, and M. V. Romalis, *Phys. Rev. Lett.*, **94**, 060801 (2005).
- [25] G. Park, C. Cunningham, B. Cabrera, and M. Huber, *Phys. Rev. Lett.* **68**, 1920 (1992).
- [26] E. Simanek, *Phys. Lett. A* **194**, 323 (1994); L. Janson, *Am. J. Phys.* **80**, 133 (2012).
- [27] S. J. Barnett, *Phys. Rev.* **6**, 239 (1915).